Optica Applicata, Vol. LIII, No. 1, 2023
DOI: 10.37190/oa230102

In-fiber Mach–Zehnder interferometer based on polarization-maintaining fiber for displacement and temperature sensing

JUN-NI CHENG, XIAO-YAN JIANG

Department of Energy Engineering of Yulin University, Yulin, Shaanxi, 719000, China

A displacement sensor based on polarization-maintaining fiber has been proposed and proved in experiment. The polarization-maintaining fiber (PMF) is sandwiched with two graded-index multimode fibers (GI MMF), which form the Mach–Zehnder interferometer (MZI) sensor. Graded -index multimode fiber serve as an optical coupler for modes conversion. The results show that with the increase of displacement, the spectrum moves to the long wavelength direction, but when temperature increases, the spectrum has a red shift, which means that the displacement and temperature can be measured separately according to the wavelength drift direction. The sensor consists of 4 mm GI MMF and 14 mm PMF, which can exhibit the displacement sensitivity of –9.275 pm/μm in the range of 0–600 μm. In addition, temperature will also affect the sensitivity of displacement measurement, so the sensitivity of the sensor to temperature is also measured. The results show that the selected monitoring dip provides a better temperature sensitivity of 33.605 pm/°C in the range of 35–75°C. The sensor is easy to fabricate and does not has any functional coating, which make it become a good candidate in the industrial field.

Keywords: displacement sensing, polarization-maintaining fiber, graded-index multimode fiber, Mach –Zehnder interferometer

1. Introduction

Displacement is the offset of the object position from the reference point. Displacement measurement technology is the basis of vibration, pressure and flow measurement technology. Compared with other mechanical quantities, displacement is easy to detect and obtain high-precision detection results. Therefore, the method of converting the mechanical quantity of the measured object into displacement is often used in measurement. At present, mechanical displacement measuring instruments are common in the industrial field, which often amplify and measure the displacement with mechanical transmission mechanism. The above methods have their own advantages and disadvantages. For example, the mechanical type has a large measurement range, and some can reach high precision, but most of them cannot be used in the production process. For displacement measurement in narrow space, the above methods have the disadvantages of large sensor volume and long probe [1,2].

In recent years, more and more attention has been paid to the measurement of object displacement with high precision and high speed, especially the measurement of small displacement in narrow space. Therefore, there are more and more displacement measurement methods using optical methods, especially the displacement measurement method using optical fiber sensing technology with unique advantages has attracted much attention. Fiber sensor because of its excellent advantages has generated huge interest in wide ranging applications [3]. Through various scientific and technological means, the performance of fiber sensors has been further studied. Many valuable results have been obtained, and the performance of sensors has been improved. As a result, the quality and application range have been improved and expanded [4–7]. Fiber based photoelectric materials and devices have been widely studied and applied in applications such as displacement detectors [8]. PULLTEAP *et al*. [9] demonstrated displacement detectors based on constructing a double cavity inside the sensing arm of F-P interferometer to realize dynamic displacement measurement. When the displacement is changed in the range of 0.7–140 μm, the measurement resolution of the sensor is 20 nm. CHEN *et al*. [10] proposed the displacement measurement based on the double -taper Mach–Zehnder interferometer. The sensor has high sensitivity but the measurement range is small. ZHOU *et al*. [11] proposed a displacement sensor based on single -mode–multi-mode–single-mode fiber structure. The wavelength shift of the interference spectrum is larger in the displacement range of 0–320 μm, but the sensor has a problem that cross-sensitivity between displacement and temperature has not been solved. These experimental findings suggest that the optical characteristics of fiber sensors play a very important practical role in the application of displacement detectors.

In this paper, we demonstrate a simple and reliable way for displacement sensing, the sensing structure and the optical properties are studied and discussed with an objective of contributing in the displacement measurement device research and application.

2. Sensor fabrication and principle

In-fiber Mach–Zehnder interferometer (MZI) is shown in Fig. 1. The core and cladding diameters of PMF and GI MMF are 9/125 μm and 50/125 μm, respectively. The graded-index multimode fibers (GI MMF) is sandwiched in a section of SMF and PMF, and the fiber taper is made at the connection between the GI MMF and input SMF by using fusion machine. The fiber taper can increase the cladding mode energy, GI MMF plays

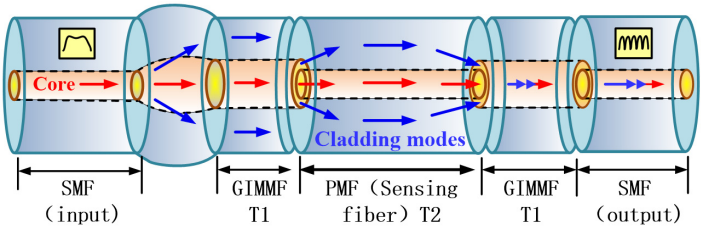

Fig. 1. Schematic diagram of the proposed interferometer.

the role of core cladding mode coupling and re-coupling, and the polarization-maintaining fiber (PMF) is used as the sensing arm. This is because PMF has the advantages of good uniformity, high strength, uniform geometric dimension, small tolerance and so on. PMF is a kind of high stress fiber. In the stress action zone of PMF, B_2O_3 is doped with the material with a thermal expansion coefficient greater than SiO_2. Due to the stress action zone, PMF is not circularly symmetrical, the fiber core is subjected to tensile stress in the direction of stress action zone, and the fiber core is subjected to compressive stress in the direction orthogonal to it. This stress will cause the refractive index of the core to change in both directions, forming the anisotropy of the refractive index in both directions. The fiber taper is welded by a commercial welding machine. After many wrong debugging and attempts, the optimal parameters of the fiber taper production are obtained: the first discharge intensity is +120, the discharge time is 300 ms. And the second discharge intensity is +150, and the discharge time is 1600 ms.

Figure 2 is a photograph of the fabricated fiber taper by using the fusion parameter. The diameter of the fiber taper is in the range of 173–179 μm. According to the coupled mode theory, the higher-order mode excitation of GI MMF section is caused by the phase matching condition $\cos^2(kT_1)$, where k is the coupling coefficient between the core mode and cladding modes, and T_1 is the length of GI MMF. GI MMF with different lengths will interfere with the excitation of other cladding modes and also affect the transverse field distribution at the interface between the sensing arm and GI MMF, and further affecting the coupling strength of cladding modes and the core mode. Therefore, through repeated experiments, the length T_1 of GI MMF is fixed to 4 mm, which help to produce relatively high fringe contrast, uniform interference spectrum and low intensity loss. The GI MMF couples a portion of the core-guided fundamental mode and re-couples to the PMF cladding through the mismatched core cross-section. At the same time, compared with the standard SM and GI MM fibers, the diameter of the fabricated fiber is larger. Reference [12] shows that using fiber taper can greatly increase the cladding mode energy, and enhance the strength of cladding mode. Light is emitted from the broadband light source. When passed through the fiber taper, part of the light will be coupled into the GI MMF core, and another part of the light will enter the GI MMF cladding. When the light transmitted passes through the PMF, due to the mismatch of

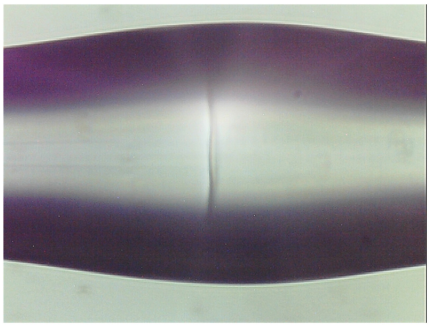

Fig. 2. Microscopic top view image of the taper.

the core, some light enters the PMF core and another light enters the PMF cladding, which means that the high-order modes in the cladding are excited. Meanwhile, the cladding modes and the core mode are met and coupled into GI MMF core. Because the effective refractive index of PMF core and cladding is different, the phase difference between the two beams of light is also caused, which results in the interference phenomenon.

When light passes through the sensor, owing to the fact that the refractive index of the core and cladding is different, the phase difference between the two beams of light will occur. The phase difference $\Delta\upsilon$ is expressed as [13]

$$\Delta\upsilon = \frac{2\pi\Delta n_{\text{eff}} L}{\lambda} \tag{1}$$

where Δn_{eff} respects effective refractive index difference between interference modes, L is PMF length in the sensor.

When the sensor is bent in the axis direction, the bending degree has a significant effect on the transmission spectrum response. WU *et al*. [14] proposed a three-dimensional simulation based on the beam propagation method to simulate the transmission characteristics of the bending part of the sensor. The results show that the refractive index of the sensing arm is isotropic distribution before the bending. Once it exceeds the bending at the point, the refractive index distribution is no longer symmetrical, which also leads the fact that the mode of excitation in the bending part is no longer symmetrical distribution [15]. Owing to the sensor different displacements, the coupling between core modes and cladding modes is also changed [16]. When the external temperature remains unchanged, the wavelength shifts of interference spectrum caused by the change of displacement can be expressed as [17]

$$\Delta\lambda_{\text{m}} = \frac{2(\Delta n_{\text{eff}} + \Delta n)L}{2k+1} - \frac{\Delta n_{\text{eff}} L}{2k+1} = \frac{2\Delta nL}{2k+1} \tag{2}$$

where $\Delta\lambda_{\text{m}}$ is the wavelength shift of the interference fringe, Δn is the variation of the effective refractive index difference between the interference modes, and k is an integer. As can be seen from Eq. (2), the wavelength drift $\Delta\lambda_{\text{m}}$ is related to the length of PMF and Δn. The bigger the sensor produces displacement, the greater the bending will become. According to the mode dispersion curve, the core refractive index and cladding refractive index can be increased. Due to the refractive index of protruding pare of bending PMF will be higher than that of depressed part, the increase of refractive index of cladding mode is larger than that of core mode, so the effective refractive index difference is negative, and the interference spectrum also shifts. The displacement can be measured by monitoring the wavelength shift of interference spectrum. When PMF is bent, a part of its internal polarized light will be coupled to its orthogonal polarization stage, which leads to the coupling of two polarization modes energy and makes the intensity of transmission spectrum change regularly [18]. Therefore, the displacement measurement can be realized by monitoring the intensity and wavelength

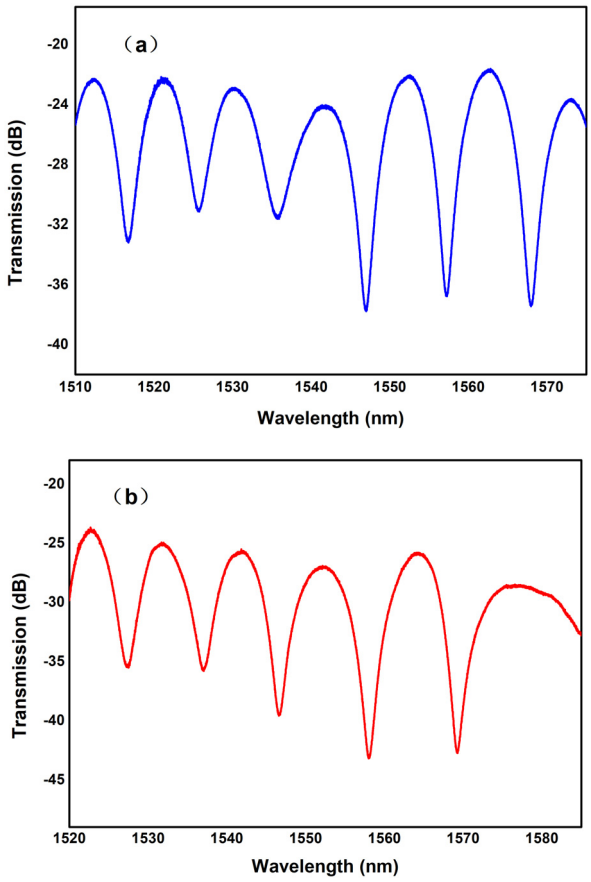

Fig. 3. Interference patterns of the fabricated interferometer: (a) S-1 and (b) S-2.

changes. In the paper, the displacement is measured by monitoring the wavelength drift in order to observe the direction of wavelength drift and realize the measurement of displacement and temperature with two parameters.

For sensor S-1 and sensor S-2, except that the PMF length is different, others are the same, including GI MMF length, the fiber taper welding parameters, *etc*. The PMF length of sensor S-1 is 10 mm and that of sensor S-2 is 14 mm, and transmission spectrum of sensors S-1 and S-2 are shown in Fig. 3.

As can be seen from Fig. 3, with the increase of PMF length, the number of interference periods in the transmission spectrum will increase, which means that the fringe spacing decreases. When the phase difference Δv is $(2k + 1)\pi$, a series of minimum values appear in the transmission spectrum. The fringe spacing $\Delta\lambda$ can be obtained from Eq. (1)

$$\Delta\lambda = \frac{\lambda^2}{\Delta n\, L} \tag{3}$$

Equation (3) shows that with the increase of PMF length L, the fringe spacing decreases gradually. This also indicates that the number of interference periods increases gradually, which is consistent with the experimental results. Through a lot of experiments, it can be found that the proposed MZI sensor can form clear interference fringes. At the same time, the extinction ratio of interference spectrum fringe is large and reaches more than 10 dB, which meets the actual measurement requirements.

To further theoretically analyze the main modes of interference in M-Z interferometer, the fast Fourier transform (FFT) is applied to the transmission spectra of sensors S-1 and S-2, as shown in Fig. 4. The spatial spectrum is [19]

$$\varepsilon = \frac{\Delta m_{\text{eff}} L}{\lambda^2} \tag{4}$$

where

$$\Delta m_{\text{eff}} = \Delta n_{\text{eff}} - \lambda_0 \frac{\partial}{\partial \lambda} \Delta n_{\text{eff}}$$

means effective refractive index difference, λ represents the central wavelength of monitoring point. As can be seen from Fig. 4, there are several peaks in the spatial spectrum of sensor S-1 and S-2, which indicates that multiple modes are involved in the interference. With the spatial frequency increasing, each spectrum exhibits a predominant peak situating at 0.0492 and 0.0752 nm^{-1} severally. At the same time, there are some lower peaks, and the corresponding frequency is larger than the corresponding frequency of the main peak, which shows that the sensor interference mode is very stable in the process of interference. As can be seen from Fig. 4, the spatial frequency of the sensor S-2 is larger than that of the sensor S-1, because the sensor S-2 has bigger length than that of the sensor S-1. According to the theoretical analysis of Eq. (4), the spatial frequency of sensor S-2 is larger than that of sensor S-1, which is consistent

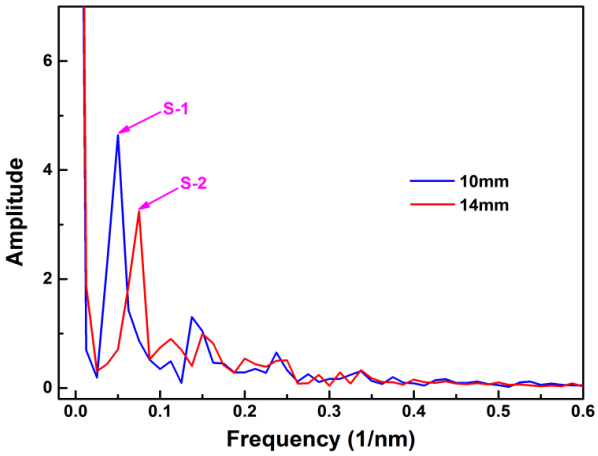

Fig. 4. Spatial frequency spectrum of the sensor in the air.

with the experimental results. Because higher-order cladding modes correspond to higher spatial frequencies, the low-order cladding modes play an important role in the inter-mode interference. Therefore, it can be considered that the interference pattern of the sensor is mainly formed by an excitation of low-order cladding mode and fundamental mode.

3. Experiment and result analysis

The schematic diagram of displacement measurement system is shown in Fig. 5 and the coordinate axis is only to calibrate the moving direction of the horizontal micrometer. Sensor S-1 and S-2 are placed in the temperature controller to measure the displacement spectral response at different temperatures. It consists of broadband light source (BBS), two-dimensional adjuster and spectral analyzer (Optical Solution Analyzer, OSA). The minimum resolution of the spectrometer is 50 pm. In the experiment, A is an adiabatic rod located at the midpoint of the PMF and closed to the lower surface of the sensor. The diameter of A is 1.5 mm. In order to eliminate the sensor loss caused by bending before the start of the experiment, the pre-stressing force is applied to the sensor at both ends. The horizontal micrometer is used to adjust the two-dimensional adjusting frame. One frame is held, and the other is moved in the negative direction of the *Z*-axis. When one frame moves from point B to C, the PMF is bent around point A. When the frame is moved, different displacements and the transmittance spectral response can be recorded. The initial distance between two ends of the two-dimensional regulator is 125 mm. The frame moves 100 μm at a time.

Figure 6 is the measurement spectra of sensors S-1 and S-2 at different temperatures with displacements of 0, 200, 500 and 600 μm. In the experiment, the dip at 1521.89 and 1521.68 nm were selected as the monitoring objects for the sensors S-1 and S-2,

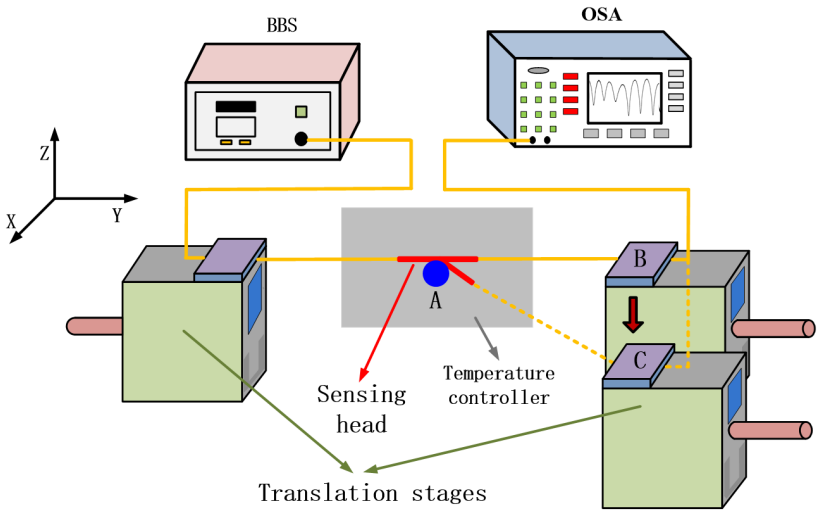

Fig. 5. The schematic diagram of the displacements measuring system.

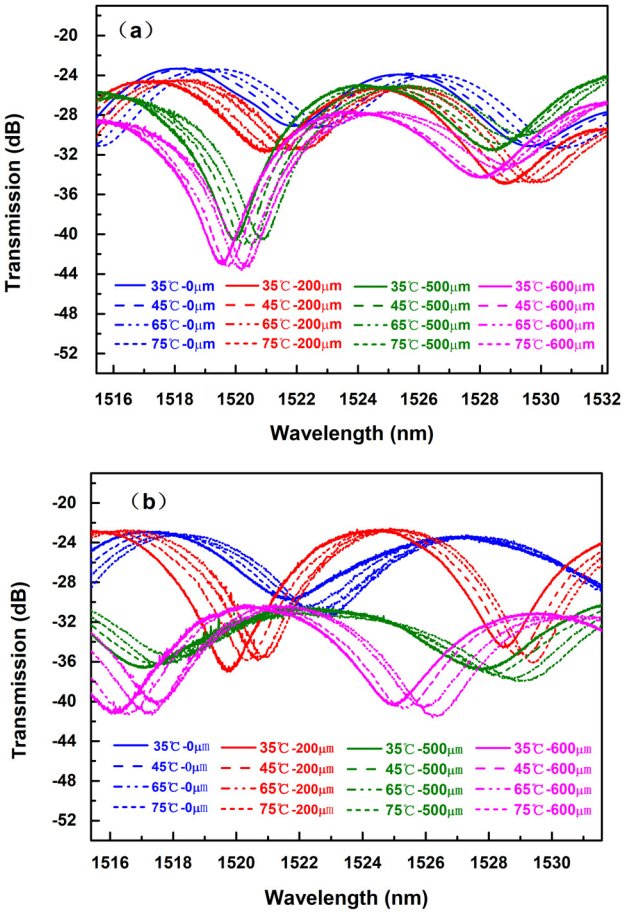

Fig. 6. Spectral responses of the sensor with different temperatures and displacements: (a) S-1 and (b) S-2.

respectively. As can be seen from Fig. 6, when the temperature remains unchanged, but the displacement increases, the transmission spectra of the sensors S-1 and S-2 exhibit blue-shift, which are in good agreement with the theoretical analysis. On the other hand, it can be seen clearly that when the displacement of the sensor remains unchanged, the transmission spectra of the sensor S-1 and S-2 show red-shift with the increasing of temperature. The reason originates from the effective refractive index difference and the length of the sensor changed, which can be due to the thermal-optic effect and thermal expansion effect, which leads to the red shift of the interference spectrum. Meanwhile, one thing can still be noticed from Fig. 6 that with the increase of temperature and displacement, wavelength shift of monitoring point presents a different direction evidently, implying that displacement and temperature can be measured independently at the same time by monitoring the direction of wavelength drift.

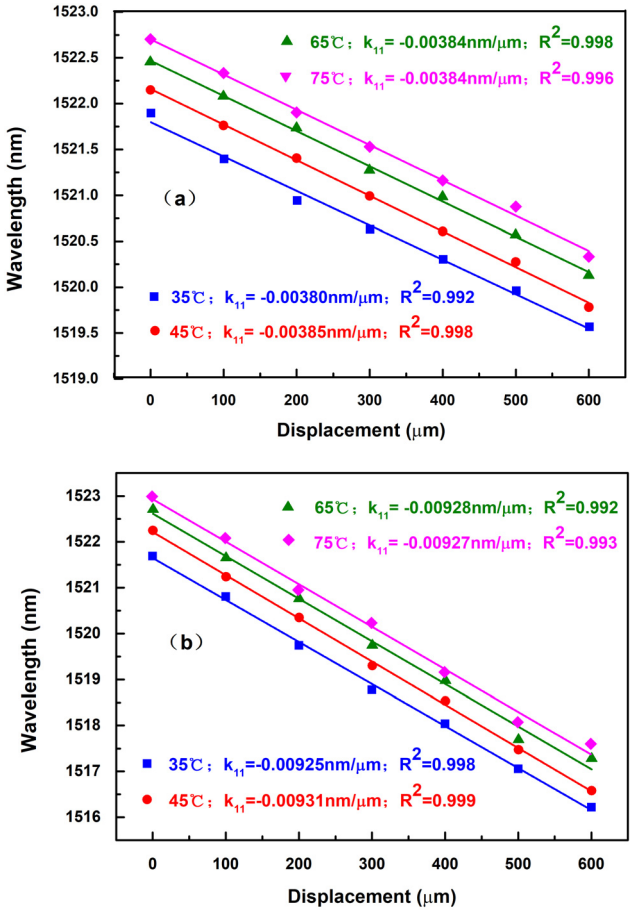

Fig. 7. The relationship between wavelength and displacement: (a) S-1 and (b) S-2.

Figure 7 shows the variation of sensor S-1 and S-2 interference spectrum wavelength and displacement at 1521.89 and 1521.68 nm, respectively. It can be seen that when the external temperature is controlled at 35–75°C, the displacement increases from 0 to 600 μm, the trough wavelength of the S-1 and S-2 monitoring points drifts to the short wave direction. The displacement response sensitivities of sensor S-1 and S-2 are varied within the scope of –3.825 ± 0.025 pm/μm and –9.275 ± 0.025 pm/μm, respectively, and the wavelength drift has a good linear relationship with the displacement.

Figures 8 and 9 show the variation of sensor S-1 and S-2 interference spectrum wavelength and temperature at 1521.89 and 1521.68 nm, respectively. When the displacement remains unchanged, the wavelength of the monitoring point drifts to the long -wave direction with the temperature risen in the range of 35–75°C. The transmission spectrum of the sensor S-1 and S-2 changes in the range of 20.605 ± 0.335 pm/°C and

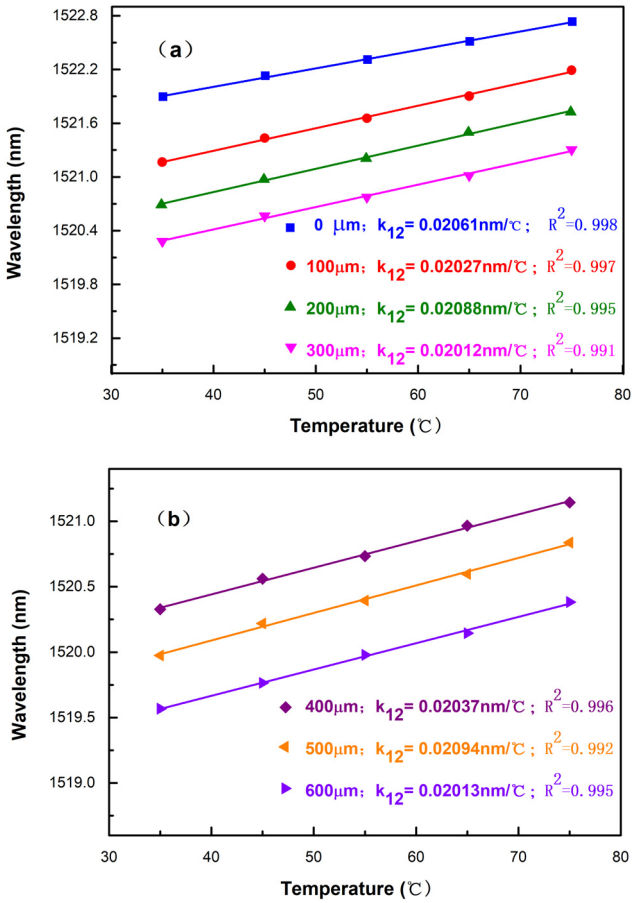

Fig. 8. The relationship between wavelength and temperature of sensor S-1.

33.605 ± 1.025 pm/°C, respectively, and the wavelength drift has a good linear relationship.

From the above analysis, it can be seen that the wavelength changes of sensor S-1 and S-2 are linearly related to displacement and temperature, so the wavelength drift caused by displacement and temperature can be expressed by a two-parameter matrix [13]

$$\begin{bmatrix} \Delta\lambda_{\text{S-1}} \\ \Delta\lambda_{\text{S-2}} \end{bmatrix} = \begin{bmatrix} K_{11,\text{ S-1}} & K_{12,\text{ S-1}} \\ K_{11,\text{ S-2}} & K_{12,\text{ S-2}} \end{bmatrix} \begin{bmatrix} \Delta D \\ \Delta T \end{bmatrix} \tag{5}$$

where the $\Delta\lambda_{\text{S-1}}$ and $\Delta\lambda_{\text{S-2}}$ are the wavelength drift of the sensor S-1 and S-2, the displacement sensitivity of the sensor S-1 and S-2 are $K_{11,\text{ S-1}}$ and $K_{11,\text{ S-2}}$, respectively.

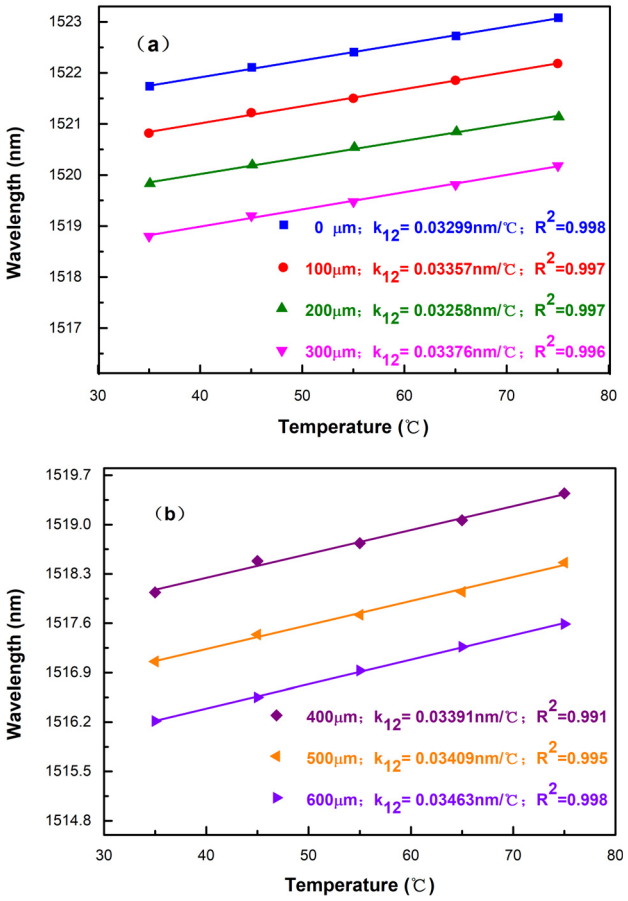

Fig. 9. The relationship between wavelength and temperature of sensor S-2.

$K_{12,\text{ S-1}}$ and $K_{12,\text{ S-2}}$ are the temperature sensitivity of the sensor S-1 and S-2, ΔD is the displacement change, and ΔT is the temperature change.

The sensitivity coefficients of displacement and temperature response measured are substituted into Eq. (5). It is shown that:

$$\begin{bmatrix} K_{11,\text{ S-1}} & K_{12,\text{ S-1}} \\ K_{11,\text{ S-2}} & K_{12,\text{ S-2}} \end{bmatrix} = \begin{bmatrix} -3.825 \pm 0.025\ \text{pm/μm} & 20.605 \pm 0.335\ \text{pm/°C} \\ -9.275 \pm 0.025\ \text{pm/μm} & 33.605 \pm 1.025\ \text{pm/°C} \end{bmatrix} \quad (6)$$

It can be seen from the Eq. (6) that there are errors under different displacements and temperatures. This is mainly due to the error brought by the experimenter during the experiment, the non-uniformity of the measured ambient temperature and the accidental error caused by the sensor displacement. In order to reduce the error, the average value can be obtained through multiple experiments.

4. Conclusion

A novel MZI sensor based on fiber taper cascading with core mismatch is proposed in this paper. Panda polarization-maintaining fiber is sandwiched in two graded-index multimode fibers to form an all-fiber MZI sensor. The light transmission theory of the sensor is analyzed, and the sensing characteristics of displacement and temperature change are studied. The experimental results show that when the displacement varies in the range of 0–600 μm, the displacement sensitivity is –9.275 pm/μm, and when the temperature varies in the range of 35–75°C, the sensitivity is 33.605 pm/°C. Moreover, experimental results indicate that with the increase of the displacement and temperature, the transmission spectrum wavelength shifts in different directions, which demonstrates its potential for the measurement of displacement and temperature with two parameters. Additionally, this type of a sensor is easily fabricated, making it a candidate in engineering field.

Acknowledgments
This work is supported by the Research Foundation of Science and Technology Board of Yu lin (2021HX350) and the Science and Technology Commission of Yu lin, Shaanxi(CXY-2020).

Reference

[1] HO D.D., HUYNH T.C., LUU T.H.T., LE T.C., *Electro-mechanical impedance-based prestress force monitoring in prestressed concrete structures*, [In] T.Q. Bui, L.T. Cuong, S. Khatir [Eds.] *Structural Health Monitoring and Engineering Structures*, Lecture Notes in Civil Engineering, Vol. 148, Springer, Singapore 2021: 413–423, DOI: 10.1007/978-981-16-0945-9_33.

[2] ZHOU Y., ZHAO C., SHI F., LI Y., DONG X., *Angle sensor with two cascading abrupt-taper based on interferometer and single mode optical fiber*, Journal of Shanghai University (Natural Science), 2017: 1–6.

[3] GAN W., ZHANG C., DAI Y., LIU F., *Design and application of the displacement sensor based on fiber Bragg grating*, Semiconductor Optoelectronics **33**(6), 2012: 795–798.

[4] ZHU Y., SHUM P., LU C., LACQUET M.B., SWART P.L., CHTCHERBAKOV A.A., SPAMMER S.J., *Temperature insensitive measurements of static displacements using a fiber Bragg grating*, Optics Express **11**(16), 2003: 1918–1924, DOI: 10.1364/OE.11.001918.

[5] SHEN C., ZHONG C., *Novel temperature-insensitive fiber Bragg grating sensor for displacement measurement*, Sensors and Actuators A: Physical **170**(1–2), 2011: 51–54, DOI: 10.1016/j.sna.2011.05.030.

[6] Zou Y., Dong X., Lin G., Adhami R., *Wide range FBG displacement sensor based on twin-core fiber filter*, Journal of Lightwave Technology **30**(3), 2012: 337–343, DOI: 10.1109/JLT.2011.2181334.

[7] RONG Q., QIAO X., ZHANG J., WANG R., HU M., FENG Z., *Simultaneous measurement for displacement and temperature using fiber Bragg grating cladding mode based on core diameter mismatch*, Journal of Lightwave Technology **30**(11), 2012: 1645–1650, DOI: 10.1109/JLT.2012.2188094.

[8] WANG Y., ZHAO C.L., HU L., DONG X., JIN Y., SHEN C., JIN S., *A tilt sensor with a compact dimension based on a long-period fiber grating*, Review of Scientific Instruments **82**(9), 2011: 093106, DOI: 10.1063/1.3639875.

[9] PULLTEAP S., SEAT H.C., *An extrinsic fiber Fabry-Perot interferometer for dynamic displacement measurement*, Photonic Sensors **5**(1), 2015: 50–59, DOI: 10.1007/s13320-014-0209-9.

[10] CHEN N.K., FENG Z.Z., WANG J.J., LIAW S.K., CHUI H.C., *Interferometric interrogation of the inclination and displacement of tapered fiber Mach-Zehnder interferometers*, IEEE Sensors Journal **13**(9), 2013: 3437–3441, DOI: 10.1109/JSEN.2013.2265170.

[11] ZHOU D.P., WEI L., LIU W.K., LIT J.W.Y., *Simultaneous strain and temperature measurement with fiber Bragg grating and multimode fibers using an intensity-based interrogation method*, IEEE Photonics Technology Letters **21**(7), 2009: 468–470, DOI: 10.1109/LPT.2009.2013640.

[12] CHENG J.N., *Mach-Zehnder interferometer based on fiber taper and fiber core mismatch for humidity sensing*, Acta Physica Sinica **67**(02), 2018: 179–185.

[13] FU G.W., LI Q.F., LI Y.P., YANG C.Q., FU X.H., BI W.H., *Temperature insensitive curvature sensor of photonic crystal fiber based on core-offset splicing and waist-enlarged fiber taper*, Acta Optica Sinica **36**(11), 2016: 1106007, DOI: 10.3788/aos201636.1106007.

[14] WU Q., HATTA A.M., WANG P., SEMENOVA Y., FARRELL G., *Use of a bent single SMS fiber structure for simultaneous measurement of displacement and temperature sensing*, IEEE Photonics Technology Letters **23**(2), 2011: 130–132, DOI: 10.1109/LPT.2010.2093515.

[15] SCHERMER R.T, COLE J.H., *Improved bend loss formula verified for optical fiber by simulation and experiment*, IEEE Journal of Quantum Electronics **43**(10), 2007: 899–909, DOI: 10.1109/JQE.2007.903364.

[16] LI B., JIANG L., WANG S., ZHOU L., XIAO H., TSAI H.-L., *Ultra-abrupt tapered fiber Mach-Zehnder interferometer sensors*, Sensors **11**(6), 2011: 5729–5739, DOI: 10.3390/s110605729.

[17] FU X.H., XIE H.Y., ZHU H.B., FU G.W., BI W.H., *Experimental research of curvature sensor based on tapered photonic crystal fiber Mach-Zehnder interferometer*, Acta Optica Sinica **35**(5), 2015: 78–83.

[18] SU Y., ZHU Y., ZHANG B., ZHOU H., LI J., WANG F., *Spectral characterization of polarization dependent loss in fiber Bragg grating under local pressure and the analysis of secondary peak*, Optical Fiber Technology **24**, 2015: 77–83, DOI: 10.1016/j.yofte.2015.05.005.

[19] CHENG J., *In-fiber Mach–Zehnder interferometer based on multi-core microfiber for humidity and temperature sensing*, Applied Optics **59**(3), 2020: 756–763, DOI: 10.1364/AO.378696.

Received February 15, 2022
in revised form April 27, 2022